Nickel-centred proton reduction catalysis in a model of [NiFe] hydrogenase.

Deborah Brazzolotto, Marcello Gennari, Nicolas Queyriaux, Trevor R. Simmons, Jacques Pécault, Serhiy Demeshko, Franc Meyer, Maylis Orio, Artero Vincent, Carole Duboc

Published in final edited form as:
Nat Chem. 2016 November ; 8(11): 1054–1060. doi:10.1038/nchem.2575.

Nickel centred H^+ reduction catalysis in a model of [NiFe] Hydrogenase

Deborah Brazzolotto[a,b], **Marcello Gennari**[a], **Nicolas Queyriaux**[b], **Trevor R. Simmons**[b,#], **Jacques Pécaut**[c], **Serhiy Demeshko**[d], **Franc Meyer**[d,f], **Maylis Orio**[e], **Vincent Artero**[b,*], and **Carole Duboc**[a,*]

[a]Univ. Grenoble Alpes, CNRS UMR 5250, DCM, F-38000 Grenoble, France

[b]Univ. Grenoble Alpes, CNRS UMR 5249, CEA, Laboratoire de Chimie et Biologie des Métaux, F-38000 Grenoble, France

[c]Univ. Grenoble Alpes, INAC-SCIB, F-38000 Grenoble, France; CEA, INAC-SCIB, Reconnaissance Ionique et Chimie de Coordination, F-38000 Grenoble, France

[d]Institute of Inorganic Chemistry, Georg-August-University Göttingen, Tammannstrasse 4, D-37077 Göttingen, Germany

[e]Institut des Sciences Moléculaires de Marseille, Aix Marseille Université, CNRS, Centrale Marseille, ISM2 UMR 7313, 13397, Marseille, France

[f]International Center for Advanced Studies of Energy Conversion (ICASEC), Georg-August-University, D-37077 Göttingen, Germany

Abstract

Hydrogen production through water splitting is one of the most promising solutions for the storage of renewable energy. [NiFe] hydrogenases are organometallic enzymes containing nickel and iron centers that catalyze hydrogen evolution with performances that rival those of platinum. These enzymes provide inspiration for the design of new molecular catalysts that do not require precious metals. However, all heterodinuclear NiFe models reported so far do not reproduce the Ni-centered reactivity found at the active site of [NiFe] hydrogenases. Here we report a structural and functional NiFe mimic that displays reactivity at the Ni site. This is shown by the detection of two catalytic intermediates that reproduce structural and electronic features of the Ni-L and Ni-R states of the enzyme during catalytic turnover. Under electrocatalytic conditions, this mimic displays high rates for H_2 evolution (second order rate constant of 2.5 10^4 $M^{-1}s^{-1}$; turnover frequency of 225 s^{-1} at 10 mM H^+ concentration) from mildly acidic solutions.

*Correspondence should be addressed to C.D. (carole.duboc@ujf-grenoble.fr) and V.A. (vincent.artero@cea.fr).
#present address: Energy Materials Laboratory, University of East Anglia, Norwich Research Park, Norwich, Norfolk NR4 7TJ, U.K.

Author contributions. C.D. and V.A. conceived and designed the project. D.B. carried out the experimental work under the supervision of M.G. T.R.S. contributed to the synthetic work. J.P. performed X-ray analysis. F.M. and S.D. performed and analysed the Mössbauer experiments. N.Q. contributed to the analysis of the electrochemical data. M.O. carried out the theoretical calculations. C.D., V.A. and M.G. analysed and interpreted the experimental data and prepared the manuscript. All the authors reviewed and contributed to the manuscript.

Competing financial interests. The authors declare no competing financial interests.

Europe PMC Funders Author Manuscripts

The first crystallographic structure of a [NiFe] hydrogenase was reported in 1995,1 and yet after two decades of extensive research, [NiFe] hydrogenases remain one of the most investigated enzymes, reflecting the current interest in sustainable fuel production and energy storage.2 [NiFe] hydrogenase catalyses the reversible reduction of protons into hydrogen (H_2), at high rates (10^3 s^{-1}) and close to the thermodynamic equilibrium. Its active site features a unique organometallic NiFe complex, in which a {Ni(cysteinate)$_4$} centre is linked via two of its cysteine ligands to an {$Fe^{II}(CN)_2(CO)$} unit (Figure 1).1 In the last decades, there has been a general agreement that only three intermediate species are involved in that catalytic cycle. The paramagnetic Ni-C state (Ni^{III}μ(H)Fe^{II})3,4 is generated from the reaction between the resting diamagnetic Ni-SI_a state ($Ni^{II}Fe^{II}$) with one electron and one proton. Ni-C is then further reduced to yield the diamagnetic Ni-R state (Ni^{II}μ(H)Fe^{II}).5,6 Protonation of the hydride ligand in Ni-R forms H_2 heterolytically, the elimination of which restores Ni-SI_a. More recently, the paramagnetic Ni-L state ($Ni^{I}Fe^{II}$),7 which can be produced from Ni-C by photolysis at cryogenic temperatures, has been proposed to be an active intermediate between Ni-SI_a and Ni-C in the catalytic cycle (Figure 1).8,9 The nickel centre is thus the key protagonist in this mechanism. It is the sole metallic site with redox activity and has a crucial role in H^- binding, the hydride asymmetrically bridging the two metallic sites in both Ni-C and Ni-R.

Reproducing the structure and function of the active site of [NiFe] hydrogenase in artificial mimics has for many years been a key challenge for synthetic chemists motivated by its original dissymmetric structure, its peculiar reactivity and the possible technological applications of efficient hydrogen production catalysts that may be developed. Despite tremendous advances in the design of NiFe models, there is still no complex that accurately mimics the structure, function and reactivity of the active site of [NiFe] hydrogenase.10–13 The main drawback of most active mimics is that their chemistry is mainly centered on the Fe site13 or on M (M = Mn14,15 or Ru16–19) in heterodinuclear NiM models,20 but not on the Ni site as in the enzyme. For instance, Ogo and Rauchfuss have evidenced that the formation of metal-hydride species in synthetic heterodinuclear NiFe/NiRu complexes is feasible,16,21–23 but in all cases, including DFT-optimized models (DFT= Density Functional Theory),14,24 the hydride ligand is either bridging14,16,22–24 but displaced toward the Fe site, or terminal and bound to the Fe center.21,25 Recently, Rauchfuss has described a NiFe mimic displaying redox activity at the Ni site with the formation of a $Ni^{I}Fe^{II}$ species. However DFT calculations showed that in the corresponding protonated species the hydride ligand is bound to iron.26 In this context, to develop better efficient mimics of the [NiFe] hydrogenase active site the reactivity needs to be relocated to the Ni center in an adequate environment. Ligand design can thus be exploited to promote redox flexibility on the Ni site (rather than on the Fe site), while maintaining a stable dinuclear framework in various oxidation states. In that context, the bipyridine-bisthiolate ligand $(L^{N2S2})^{2-}$ (Figure 2) is particularly interesting since it forms stable nickel complexes in all three oxidation states from +I to +III.27,28 Additionally, a {FeCpCO} unit has previously been used as a surrogate for the {$FeCO(CN)_2$} moiety of the natural cluster for the successful design of synthetic mimics.29–31

Herein, we report the synthesis and analysis of a heterodinuclear NiFe complex, $[L^{N2S2}Ni^{II}Fe^{II}Cp(CO)]^+$ (**$L^{N2S2}Ni^{II}Fe^{II}$**) (Figure 2), that models the active site of [NiFe] hydrogenase and produces H_2 electrocatalytically at high rate. The present work represents a breakthrough as two derivatives that are involved as intermediates in the catalytic cycle were also isolated, which reproduce the structure and spectroscopic signatures of the Ni-R and Ni-L states, indicating that the entire catalytic cycle of **$L^{N2S2}Ni^{II}Fe^{II}$** is nickel-centered.

Results

Synthesis and characterization of $L^{N2S2}Ni^{II}Fe^{II}$, a Ni-Si_a model

$L^{N2S2}Ni^{II}Fe^{II}$ has been isolated from the reaction between the two corresponding mononuclear units (Figure 2a), i.e. the dithiolate Ni^{II} complex $[Ni^{II}L^{N2S2}]$ and the carbonyl Fe^{II} complex, $[CpFe^{II}(CO)(MeCN)_2]^+$. It mimics the Ni-$SI_a$ state of the enzyme, as its X-ray structure (Figure 2b, Supplementary Fig. 1) reveals a $\{NiFeS_2\}$ core identical to that of Ni-SI_a state with the two thiolates bridging the Ni^{II} and Fe^{II} ions and a Ni···Fe distance of 2.88(4) Å close to that (~2.8 Å) determined for Ni-SI_a through DFT calculations.32 The dinuclear structure of **$L^{N2S2}Ni^{II}Fe^{II}$** is maintained in solution, as shown by Nuclear Overhauser Effect (Supplementary Figs 2-3) and Electrospray Ionization mass experiments.

The **$L^{N2S2}Ni^{II}Fe^{II}$** complex also displays spectroscopic signatures (Figure 3) similar to those measured for Ni-SI_a: (i) from Electron Paramagnetic Resonance (EPR) and Nuclear Magnetic Resonance (NMR) measurements, **$L^{N2S2}Ni^{II}Fe^{II}$** is diamagnetic with both low-spin ($S = 0$) Ni^{II} and Fe^{II} ions as in Ni-SI_a. Accordingly, the Ni-S and Ni-N bond distances are similar to those measured in the low-spin $[Ni^{II}L^{N2S2}]$ complex;28 (ii) the Mössbauer spectrum of **$L^{N2S2}Ni^{II}Fe^{II}$** (Supplementary Fig. 4) displays a doublet with isomer shift δ = 0.39 mm·s^{-1} and quadrupole splitting ΔE_Q = 1.82 mm·s^{-1} characteristic of a low-spin Fe^{II} ion, even though the isomer shift is slightly higher than the value reported for Ni-SI_a (δ = 0.10 mm·s^{-1}, ΔE_Q = 1.60 mm·s^{-1})33; (iii) the CO stretching vibration ($\bar{\nu}_{CO}$ = 1929 cm^{-1}, Supplementary Fig. 5) of the carbonyl ligand coordinated to the Fe^{II} center is in the same range as for Ni-SI_a (1925-1956 cm^{-1}).2,34

All spectroscopic parameters are well reproduced by theoretical calculations performed on the optimized **$L^{N2S2}Ni^{II}Fe^{II}$*** structure using the DFT approach (Figure 3, optimized structures are indicated with an asterisk throughout the manuscript), demonstrating the viability of our theoretical approach for further analysis.

In brief, despite some variations in the metal coordination spheres, the structural and spectroscopic properties closely resemble those of the enzyme's active site. The two terminal Ni-bound thiolates have been replaced by a bipyridine unit providing rigidity and preorganization essential for active catalysis and acting as an electron reservoir (see below), thus mimicking the proximal [4Fe4S] cluster. Essentially, the $(L^{N2S2})^{2-}$ ligand affords an unsaturated four-coordinated Ni^{II} site appropriate for Ni-centered reactivity, as in the enzyme.

Redox properties of $L^{N2S2}Ni^{II}Fe^{II}$

The cyclic voltammogram (CV) of $\mathbf{L^{N2S2}Ni^{II}Fe^{II}}$ recorded in MeCN (Figure 4) displays two reversible and diffusion controlled one electron reduction waves at –1.29 V and –1.90 V *vs* Fc^+/Fc (Supplementary Fig. 6). These waves can be assigned to the successive reductions of the Ni^{II} to Ni^{I} (formation of $\mathbf{L^{N2S2}Ni^{I}Fe^{II}}$) and of the bipyridine moiety in $(L^{N2S2})^{2-}$ as attested by a DFT optimized structure of $\mathbf{L^{N2S2\bullet}Ni^{I}Fe^{II}}$ displaying a strong radical character on the bipyridine bound to the Ni^{I} site (Supplementary Fig. 7). A similar redox behaviour has previously been observed in a diiron mimic of the active site of the [FeFe]-hydrogenase containing a bipyridine ligand.35

The reversible electrochemical behaviour of $\mathbf{L^{N2S2}Ni^{II}Fe^{II}}$ is unprecedented among NiFe mimics, which generally displayed irreversible reduction processes, indicating strong structural reorganisation at the metal site(s) possibly accompanied by ligand degradation *via* radical processes. The large anodic shift (530 mV) of the Ni^{II}/Ni^{I} redox potential in $\mathbf{L^{N2S2}Ni^{II}Fe^{II}}$, compared to $[Ni^{II}L^{N2S2}]$ ($E_{1/2}$ = -1.82 V),21 nicely illustrates how the electronics of the nickel center can be modulated by the organometallic iron unit, in a similar fashion to the active site of [NiFe] hydrogenases. The linkage of the cationic Fe moiety bearing the strong π-acceptor CO ligand withdraws electron density through thiolate ligands, which acquire thioether-like electronic properties.36

Electrocatalytic activity of $L^{N2S2}Ni^{II}Fe^{II}$ for H_2 production

Upon addition of Et_3NHBF_4 as a proton source (pKa = 18.6 in MeCN),37 a catalytic process (E_{cat} = –1.90 V vs Fc^+/Fc, measured at the half-wave) develops on the top of the second reversible wave (Figure 4 and Supplementary Fig. 8). Bulk electrolysis experiments performed at –1.85 V on Hg-pool cathode confirm electrocatalytic production of H_2 (16 turnovers achieved, 70% conversion within 100 minutes) with faradic yields of 70 % from Et_3NHBF_4 (50 equiv.) solution in the presence of $\mathbf{L^{N2S2}Ni^{II}Fe^{II}}$ (Supplementary Fig. 9). While the mononuclear Fe^{II} precursor, $[CpFe^{II}(CO)(MeCN)_2]^+$, displays no reactivity toward protons under similar conditions, $[Ni^{II}L^{N2S2}]$ produces H_2 but to a lesser extent (9 turnovers achieved within 100 minutes). When electrocatalytic studies are carried out on GC electrode, rinse test experiments and Scanning Electron Microscopy confirmed that no surface-confined species are responsible for the observed catalytic activity (Supplementary Information Figs 10 and 11).

To gain more insight into the kinetics of the electrocatalytic hydrogen production, foot-of-the-wave (FOWA) analysis has been carried out38 and allowed for a second-order rate constant (k_{cat}) of 2.5 ± 0.3 10^4 $M^{-1}\cdot s^{-1}$ to be determined (Supplementary Fig. 12), which ranks $\mathbf{L^{N2S2}Ni^{II}Fe^{II}}$ high in the series of H_2-evolving systems for which such rate constants were measured (10^6 - 10^4 $M^{-1}\cdot s^{-1}$ range, the best being iron-porphyrin).14,39–41 For comparison, under the same conditions the mononuclear $[Ni^{II}L^{N2S2}]$ catalyst gives a k_{cat} value of 2.2± 0.3 10^3 $M^{-1}\cdot s^{-1}$, that is one order of magnitude lower than that of $\mathbf{L^{N2S2}Ni^{II}Fe^{II}}$. From these numbers and the conditions used for bulk electrolysis experiments, turnover frequency (TOF) values of 225 s^{-1} and 20 s^{-1} can be determined for $\mathbf{L^{N2S2}Ni^{II}Fe^{II}}$ and $[Ni^{II}L^{N2S2}]$, respectively. These values reflect the intrinsic activity of the catalysts. They are significantly larger than those tentatively derived from bulk electrolysis

experiments. Such a discrepancy arises from the fact that not all the catalyst present in the bulk solution is active but only the fraction present in the convection-reaction layer at the immediate vicinity of the electrode. In addition, the current measured during bulk electrolysis experiments is limited by mass transport and consumption of the proton source.

The experimentally determined k_{cat} value of $\mathbf{L^{N2S2}Ni^{II}Fe^{II}}$ translates into an extrapolated TOF_{max} value of 2.5 10^4 s^{-1} in 1M acid solution (the standard condition proposed for a rational benchmark of performances of H_2 evolution catalysts using catalytic Tafel plot) assuming that the reaction remains first order in acid.39 Based on an EECC mechanism (as proposed below) together with a E_{cat} value of –1.90 V and an apparent equilibrium potential of the H^+/H_2 couple (–1.21 V), we could depict the red trace in the catalytic Tafel plot shown in Figure 4, relating turnover frequency and driving force of the reaction, i.e. the overpotential related to H_2 evolution under the conditions used.39 Although not rivaling DuBois' bioinspired Ni complexes,42 our novel $\mathbf{L^{N2S2}Ni^{II}Fe^{II}}$ complex displays significant catalytic activity ($\log(TOF/s^{-1})>1$) for overpotential values larger than 500 mV and therefore compares well with other electrocatalysts based on non-noble metals,39,43 including FeTPP,40 a mononuclear Mn complex41 or a $Ni^{II}Mn^{I}$ mimic14 of the active site of [NiFe] hydrogenase.

Characterization of $L^{N2S2}Ni^{I}Fe^{II}$, an active Ni-L model

With the aim of better understanding the electrocatalytic mechanism of H_2 production, efforts have been carried out to generate and characterize potential intermediate species. First, we isolated the one-electron reduced form of $\mathbf{L^{N2S2}Ni^{II}Fe^{II}}$. We have observed that this species adsorbs at the surface of GC electrodes in the course of bulk electrolysis experiments performed in wet MeCN ($[H_2O] > 0.5$ M) electrolyte. This reduced species can be redissolved in THF and displays the same spectroscopic properties that the powder obtained from the reaction of a MeCN solution of $\mathbf{L^{N2S2}Ni^{II}Fe^{II}}$ with 1 equiv. of cobaltocene (Supplementary Figs 5, 13, 14).

This paramagnetic species has been assigned to the $[L^{N2S2}Ni^{I}\mu(CO)Fe^{II}Cp]$ complex, $\mathbf{L^{N2S2}Ni^{I}Fe^{II}}$, based on several spectroscopic results (Figure 3). The $S = ½$ EPR signature of the $\mathbf{L^{N2S2}Ni^{I}Fe^{II}}$ solution exhibits a characteristic axial signal of a Ni^{I}-based compound ($g_{\parallel} = 2.168$, $g_{\perp} = 2.060$, Supplementary Fig. 13). The Mössbauer doublet displays similar δ and ΔE_Q parameters to those of the initial $\mathbf{L^{N2S2}Ni^{II}Fe^{II}}$ complex demonstrating that the Fe site remains a low spin Fe^{II} ion with a similar coordination sphere (Supplementary Fig. 4). The CO vibration wavenumber is shifted to 1770 cm^{-1} in agreement with a CO bridging the Fe and Ni ions (Supplementary Fig. 5). Another minor side-product co-precipitates with $\mathbf{L^{N2S2}Ni^{I}Fe^{II}}$ and has been assigned to the aquo adduct $[L^{N2S2}Ni^{I}(OH_2)Fe^{II}Cp(CO)]$, as detailed in the Supplementary Information.

The $[L^{N2S2}Ni^{I}\mu(CO)Fe^{II}Cp]$ structure of $\mathbf{L^{N2S2}Ni^{I}Fe^{II}}$ has been confirmed by DFT calculations. All spectroscopic parameters calculated on its optimized structure ($\mathbf{L^{N2S2}Ni^{I}Fe^{II}*}$) are in reasonable to excellent agreement with the experimental data (Figure 3). Upon reduction, the Ni···Fe distance is shortened to 2.52 Å likely due to the presence of the bridging carbonyl (Ni-CO: 2.064 Å and Fe-CO: 1.803 Å). In Ni-L, it has been evidenced that the short Ni-Fe distance arises from a metal-metal bond (2.56 Å).44 Although the Ni-Fe

bond displays a Mayer bond order of 0.227 consistent with a metal-metal bond in $\mathbf{L^{N2S2}Ni^{I}Fe^{II}*}$, a Natural Bond Order (NBO) analysis was carried out to obtain an unequivocal representation of the Ni-Fe interaction. The corresponding natural orbital features an out-of-phase symmetry consistent with a net anti-bonding interaction between the two metals centres (Supplementary Fig. 15). The single occupied molecular orbital (SOMO, Supplementary Fig. 16) is mainly centered on the Ni ion (76 and 1 % on the Ni and Fe sites, respectively, *vs* 81 and 15 % in Ni-SI_a)44 with partial delocalization on the bipyridine moiety of $(L^{N2S2})^{2-}$ (7% on the N atoms).

While a large *g*-anisotropy is found in Ni-L (g_z = 2.046, g_y = 2.118 and g_x = 2.296 with Δg = 0.25),3 Δg values in the range 0.09-0.16 are found in the model compounds,26,45 including $\mathbf{L^{N2S2}Ni^{I}Fe^{II}}$. This discrepancy can be related to the different coordination spheres of the Ni^{I} ion. In Ni-L, the Ni^{I} ion is four-coordinate, while it is five-coordinate in the synthetic models. Stable four-coordinate Ni^{I} complexes are remarkably rare and require an appropriate ligand scaffold to avoid binding of a fifth ligand.46 In Ni-L second coordination sphere effects probably play a crucial role in favouring this arrangement. Despite this difference, $\mathbf{L^{N2S2}Ni^{I}Fe^{II}}$ represents the first mimic of the Ni-L state characterized in the context of a full catalytic cycle, which supports the fact that Ni-L is indeed an active intermediate for [NiFe] hydrogenase.9,47

Characterization of $L^{N2S2}Ni^{II}(H)Fe^{II}$ a Ni-R model

Our next attempt was focused on the detection of a metal-hydride species. When an excess of $NaBH_4$ is added to a MeCN solution of $\mathbf{L^{N2S2}Ni^{II}Fe^{II}}$, the Infra-Red (IR) spectrum of the solution displays a new CO vibration (1838 cm^{-1}), in addition to those (1770 and 1888 cm^{-1}) attributed to $\mathbf{L^{N2S2}Ni^{I}Fe^{II}}$ and its aquo adduct. While formation of $\mathbf{L^{N2S2}Ni^{I}Fe^{II}}$ simply reflects the reducing nature of BH_4^- ions, the new feature at 1838 cm^{-1}, which shifts to 1844 cm^{-1} when using $NaBD_4$, can be confidently assigned to a hydride derivative. In the ^1H NMR spectrum (Supplementary Fig. 17), a sharp peak at –6.80 ppm is observed consistent with a diamagnetic species containing a metal-bound hydride ligand, therefore named $\mathbf{L^{N2S2}Ni^{II}(H)Fe^{II}}$ hereafter. Based on the relative intensity of this peak with those accounting for $\mathbf{L^{N2S2}Ni^{I}Fe^{II}}$, $\mathbf{L^{N2S2}Ni^{II}(H)Fe^{II}}$ represents maximum 15% of the sample.

The optimized $\mathbf{L^{N2S2}Ni^{II}(H)Fe^{II}*}$ structure indicates that the hydride ligand is terminally bound to the Ni^{II} site and that the CO ligand remains terminally bound to the Fe^{II} site (Figure 3). The DFT-predicted spectroscopic parameters (IR and NMR) agree well with the experimental data. $\mathbf{L^{N2S2}Ni^{II}(H)Fe^{II}}$ thus has a composition and redox state analogous to the Ni-R state of NiFe hydrogenase.

In Ni-R, the hydride bridges the two metals dissymmetrically and is displaced toward the Ni site as revealed by the Ni-H and Fe-H bond distances of 1.58 Å and 1.78 Å, respectively.6 Interestingly, even if the hydride is terminally bound to Ni in $\mathbf{L^{N2S2}Ni^{II}(H)Fe^{II}*}$, the calculated Ni-H bond distance is similar (1.55 Å) to that in Ni-R and in the range of Ni-H length values found in the literature for terminal hydride ligands (1.33-1.65 Å).48–50 Besides, the present model reproduces the notable dissymmetry observed in Ni-R between the two Ni-$S_{bridging}$ bonds (2.54 and 2.21 Å in Ni-R and 2.30 and 2.18 Å in

$L^{N2S2}Ni^{II}(H)Fe^{II*}$). In the three previously isolated Ni-R models, the hydride ligand binds in either a terminal mode to the Fe site21 (Fe-H distance of 1.57 Å) or a dissymmetric bridging mode displaced toward the Fe ion (Δd (M-H) of 0.18 and 0.4 Å with Ni-H length of 1.64 and 1.89 Å, respectively).22,23 With this unprecedented structure, **$L^{N2S2}Ni^{II}(H)Fe^{II}$** thus represents the best active mimic of the Ni-R state involved in H_2 evolution catalysis to date.

Discussion

Based on all experimental results combined with DFT calculations, the electrocatalytic mechanism shown in Figure 5 can be proposed. **$L^{N2S2}Ni^{II}Fe^{II}$** undergoes a one-electron reduction to generate **$L^{N2S2}Ni^{I}Fe^{II}$**. This active species is further reduced to afford **$L^{N2S2\bullet}Ni^{I}Fe^{II}$**, which reacts with protons to yield **$L^{N2S2}Ni^{II}(H)Fe^{II}$**. The metal-hydride species further reacts with protons to produce H_2, and to regenerate the initial **$L^{N2S2}Ni^{II}Fe^{II}$** complex.

Such a catalytic cycle, involving decoupled electron and proton transfers, is similar to that proposed for the enzyme, except that the electron/proton transfer sequence yielding Ni-R/ **$L^{N2S2}Ni^{II}(H)Fe^{II}$** from the one-electron reduced form, Ni-L/ **$L^{N2S2}Ni^{I}Fe^{II}$** is inverted. As a consequence, the formation of a **$L^{N2S2}Ni^{III}(H)Fe^{II}$** species, analogous to Ni-C, is bypassed in our system. It is hypothesised that protonation of **$L^{N2S2}Ni^{I}Fe^{II}$** by Et_3NH^+ is either thermodynamically unfavourable or too slow to be observed on the timescale of a CV experiment. This can be rationalized by the poor basic and nucleophilic character of **$L^{N2S2}Ni^{I}Fe^{II}$**, compared to Ni-L, due to (i) a much weaker electronic donor, coordination environment ($\{N_2S_2\}^{2-}$ for Ni^I vs. $\{S_4\}^{4-}$ in the enzyme); (ii) partial delocalization of the SOMO on the bipyridine moiety of $(L^{N2S2})^{2-}$ and (iii) the absence of any proton relay that could kinetically assist protonation of the Ni^I center.

However, addition of a stronger acid such as HBF_4 (pKa = 0.1)[37] to **$L^{N2S2}Ni^{I}Fe^{II}$** in MeCN stoichiometrically yields H_2 (0.40 equiv., 80% determined by gas chromatography analysis) with the concomitant regeneration of **$L^{N2S2}Ni^{II}Fe^{II}$**. Such a reactivity suggests the transient formation of the **$L^{N2S2}Ni^{III}(H)Fe^{II}$** species under these particular conditions, which either evolves H_2 in a homolytic bimolecular fashion, or reacts with a proton to produce H_2 heterolytically after *in situ* reduction to **$L^{N2S2}Ni^{II}(H)Fe^{II}$** by a neighbouring molecule of **$L^{N2S2}Ni^{I}Fe^{II}$**. Conversely, the **$L^{N2S2\bullet}Ni^{I}Fe^{II}$** intermediate formed during the electrocatalytic pathway displayed in Figure 5, parallels the formation of a super-reduced state, implicated in the catalytic cycle of [FeFe] hydrogenase.51 In this natural super-reduced state, the additional electron is located on the proximal [4Fe4S] cluster,52,53 while in **$L^{N2S2\bullet}Ni^{I}Fe^{II}$** the bipyridine moiety acts as the electron reservoir. Whether [NiFe] hydrogenase could also exist in such a super-reduced state is an interesting question, but the present mechanism clearly demonstrates how the sequence of the various electron and proton transfer steps can be controlled in synthetic NiFe mimics through fine-tuning the redox and electronic properties of the system.

In summary, **$L^{N2S2}Ni^{II}Fe^{II}$** displays the best performance of any reported [NiFe] hydrogenase mimic to date, with regards to electrocatalytic H_2 production. It is also the first

heterodinuclear mimic, whose reactivity occurs on the Ni site. As in the enzyme, the Fe site of $\mathbf{L^{N2S2}Ni^{II}Fe^{II}}$ is involved in the modulation of the electronic properties of the {Ni(cysteinate)$_4$} site. Such a conclusion is further supported by electrolysis experiments (better H_2 production performances in terms of both efficiency and kinetics of $\mathbf{L^{N2S2}Ni^{II}Fe^{II}}$ *vs* [$Ni^{II}L^{N2S2}$]) demonstrating a cooperative effect of the Fe site on the reactivity of the {NiL^{N2S2}} unit. This work opens new avenues in the development of accurate [NiFe] hydrogenase mimics with rationally designed activity. We note that a significant improvements in the performance of [FeFe] hydrogenase mimics were achieved from 2007 onwards, after the observation that terminal hydride ligands could be isolated in FeFe complexes.54–60 We hope that the insights reported here will lead to a similar improvement in the properties of [NiFe] hydrogenase mimics.

Methods

[$Ni^{II}L^{N2S2}$] was prepared according to a previously reported procedure.28 [CpFe(CO)$_2$(MeCN)$_2$]BF_4 was prepared from [CpFe(CO)$_2$(thf)]BF_4,61 as reported in the Supplementary Information. All other reagents were used as received. All solvents were dried and distilled prior to use according to conventional methods. All reactions and manipulations were performed under inert atmosphere (argon, in a glove box or in Schlenk tubes).

Synthesis of [$L^{N2S2}Ni^{II}Fe^{II}$(Cp)(CO)]BF_4 ($L^{N2S2}Ni^{II}Fe^{II}BF_4$)

Solid [$Ni^{II}L^{N2S2}$] (100 mg, 0.157 mmol) was added to a solution of [CpFe(CO)$_2$(MeCN)$_2$]BF_4 (50 mg, 0.157 mmol) in CH_2Cl_2 (10 mL) under stirring at 20 °C. The color of the resulting solution slowly turned to dark brown. After 48 hours, diethyl ether was allowed to slowly diffuse into the reaction solution. After few days, X-ray suitable dark brown crystals, corresponding to $\mathbf{L^{N2S2}Ni^{II}Fe^{II}}BF_4{\cdot}1.5Et_2O$, were obtained. These were filtered, washed with diethyl ether and dried (121 mg, 83%). IR (cm^{-1}): 3055w, 3027w, 2350w, 1926vs, 1604m, 1488m, 1442m, 1425w, 1265w, 1053s, 1030s, 810m, 803w, 753m, 695s. ^{1}H NMR (400 MHz, CD_3CN): δ 7.87 (d, J = 7.4 Hz, 2H, CH bpy), 7.67 (t, J = 7.9 Hz, 2H, CH bpy), 7.56 (s br, 4H), 7.38 (m, 10H), 7.20 (m, 6H), 6.70 (d, J = 7.4 Hz, 2H, CH bpy), 4.11 (d, J = 13.4 Hz, 2H, CH of diastereotopic CH_2), 3.86 (d, J = 13.4 Hz, 2H, CH of diast. CH_2), 3.52 (s, 5H, CH Cp). ESI-MS ($5{\cdot}10^{-5}$ M, MeCN, m/z, I%): 785.2 100 $[M]^+$. Anal. Calcd. for $C_{44}H_{35}FeN_2NiOS_2BF_4{\cdot}0.5Et_2O{\cdot}0.9H_2O$ (926.51): C, 59.63; H, 4.55; N, 3.02; Found: C, 59.69; H, 4.38; N, 3.19.

Synthesis of [$L^{N2S2}Ni^{I}Fe^{II}$(Cp)(CO)] ($L^{N2S2}Ni^{I}Fe^{II}$)

A solution of bis(cyclopentadienyl)cobalt(II) (7.2 mg, 0.038 mmol) in MeCN (2 mL) was added to a solution of $\mathbf{L^{N2S2}Ni^{II}Fe^{II}}BF_4$ (30.0 mg, 0.034 mmol) in MeCN (2 mL) at 20 °C, yielding a black precipitate. After 15 min, it was filtered, washed with MeCN (1 mL), dried and collected as a black powder (18.0 mg, 67%). IR (cm^{-1}): 3056w, 1889w (minor species, assigned to [$L^{N2S2}Ni^{I}(OH_2)Fe^{II}$(Cp)(CO)], 1770vs, 1593w, 1487m, 1440m, 1418w, 1390m, 1080w, 1032w, 804w, 786w, 751m, 701s, 670m.

For preparative electrochemical formation of $\mathbf{L^{N2S2}Ni^{I}Fe^{II}}$, a glassy carbon foam and wet acetonitrile (0.1 M Bu_4NClO_4 and [H_2O] > 0.5 M) were used as working electrode and

electrolyte, respectively. Electrolysis was carried out for 10 min at –1.46 V vs Fc^+/Fc. $\mathbf{L^{N2S2}Ni^{I}Fe^{II}}$ was dissolved from the electrode surface through washing with THF or CH_2Cl_2. No compound could be spectroscopically detected in the washings if a dry electrolyte is used during electrolysis.

Reaction of $L^{N2S2}Ni^{II}Fe^{II}$ with $NaBH_4$

When a solution of $NaBH_4$ in MeOH or EtOH (5-20 equivalents) is added to one of $\mathbf{L^{N2S2}Ni^{II}Fe^{II}}BF_4$ (10 mM) in MeCN, a black precipitate is formed. After 3 min, it is filtered, dried and analysed by IR spectroscopy. The infrared spectrum shows a mixture of three products: $\mathbf{L^{N2S2}Ni^{I}Fe^{II}}$ (main product, peak at 1770 cm^{-1}), $[L^{N2S2}Ni^{I}(OH_2)Fe^{II}(Cp)(CO)]$ (peak at 1888 cm^{-1}), and $[L^{N2S2}Ni^{II}(H)Fe^{II}(Cp)(CO)]$ ($\mathbf{L^{N2S2}Ni^{II}Fe^{II}H}$, peak at 1838 cm^{-1}). $\mathbf{L^{N2S2}Ni^{II}Fe^{II}H}$ can be identified (and quantified) also by the presence of a singlet at -6.81 ppm (H-Ni) in the ^1H NMR spectrum in d^8-thf. Up to a ~15% of $\mathbf{L^{N2S2}Ni^{II}Fe^{II}H}$ could be detected under the present conditions.

Supplementary Material

Refer to Web version on PubMed Central for supplementary material.

Acknowledgements

Financial support for this work was provided by Labex arcane (ANR-11-LABX-003), the European Research Council under the European Union's Seventh Framework Programme (FP/2007-2013)/ERC Grant Agreement n. 306398 and the COST Action CM1305 (EcostBio) including a STSM grant (COST-STSM-CM1305- 26539) to DB.

References

1. Volbeda A, et al. Crystal structure of the nickel-iron hydrogenase from desulfovibrio gigas. Nature. 1995; 373:580–587. [PubMed: 7854413]
2. Lubitz W, Ogata H, Rüdiger O, Reijerse E. Hydrogenases. Chem Rev. 2014; 114:4081–4148. [PubMed: 24655035]
3. Foerster S, et al. Single crystal EPR studies of the reduced active site of [NiFe] hydrogenase from desulfovibrio vulgaris miyazaki F. J Am Chem Soc. 2003; 125:83–93. [PubMed: 12515509]
4. Brecht M, van Gastel M, Buhrke T, Friedrich B, Lubitz W. Direct detection of a hydrogen ligand in the [NiFe] center of the regulatory H_2-sensing hydrogenase from ralstonia eutropha in its reduced state by HYSCORE and ENDOR spectroscopy. J Am Chem Soc. 2003; 125:13075–13083. [PubMed: 14570480]
5. George SJ, Kurkin S, Thorneley RNF, Albracht SPJ. Reactions of H_2, CO, and O_2 with active [NiFe]-hydrogenase from allochromatium vinosum. A stopped-flow infrared study. Biochemistry. 2004; 43:6808–6819. [PubMed: 15157115]
6. Ogata H, Nishikawa K, Lubitz W. Hydrogens detected by subatomic resolution protein crystallography in a [NiFe] hydrogenase. Nature. 2015; 520:571–574. [PubMed: 25624102]
7. van der Zwaan JW, Albracht SPJ, Fontijn RD, Slater EC. Monovalent nickel in hydrogenase from chromatium vinosum: Light sensitivity and evidence for direct interaction with hydrogen. FEBS Lett. 1985; 179:271–277. [PubMed: 2981705]
8. Murphy BJ, et al. Discovery of dark pH-dependent H^+ migration in a [NiFe]-hydrogenase and its mechanistic relevance: Mobilizing the hydrido ligand of the Ni-C intermediate. J Am Chem Soc. 2015; 137:8484–8489. [PubMed: 26103582]
9. Hidalgo R, Ash PA, Healy AJ, Vincent KA. Infrared spectroscopy during electrocatalytic turnover reveals the Ni-L active site state during H_2 oxidation by a NiFe hydrogenase. Angew Chem Int Ed. 2015; 54:7110–7113.

10. Tard C, Pickett CJ. Structural and functional analogues of the active sites of the [Fe]-, [NiFe]-, and [FeFe]-hydrogenases. Chem Rev. 2009; 109:2245–2274. [PubMed: 19438209]
11. Ohki Y, Tatsumi K. Thiolate-bridged iron–nickel models for the active site of [NiFe] hydrogenase. Eur J Inorg Chem. 2011; 2011:973–985.
12. Simmons TR, Berggren G, Bacchi M, Fontecave M, Artero V. Mimicking hydrogenases: From biomimetics to artificial enzymes. Coord Chem Rev. 2014; 270–271:127–150.
13. Kaur-Ghumaan S, Stein M. [NiFe] hydrogenases: How close do structural and functional mimics approach the active site? Dalton Trans. 2014; 43:9392–9405. [PubMed: 24846119]
14. Fourmond V, et al. A nickel-manganese catalyst as a biomimic of the active site of NiFe hydrogenases: A combined electrocatalytical and DFT mechanistic study. Energy Environ Sci. 2011; 4:2417–2427.
15. Song L-C, Li J-P, Xie Z-J, Song H-B. Synthesis, structural characterization, and electrochemical properties of dinuclear Ni/Mn model complexes for the active site of [NiFe]-hydrogenases. Inorg Chem. 2013; 52:11618–11626. [PubMed: 24063734]
16. Ogo S, et al. A dinuclear Ni(μ-H)Ru complex derived from H_2. Science. 2007; 316:585–587. [PubMed: 17463285]
17. Canaguier S, Fontecave M, Artero V. Cp*-ruthenium-nickel-based H_2-evolving electrocatalysts as bio-inspired models of NiFe hydrogenases. Eur J Inorg Chem. 2011:1094–1099.
18. Canaguier S, et al. Catalytic hydrogen production by a Ni-Ru mimic of NiFe hydrogenases involves a proton-coupled electron transfer step. Chem Commun. 2013; 49:5004–5006.
19. Oudart Y, Artero V, Pécaut J, Lebrun C, Fontecave M. Dinuclear nickel-ruthenium complexes as functional bio-inspired models of NiFe hydrogenases. Eur J Inorg Chem. 2007:2613–2626.
20. Denny JA, Darensbourg MY. Metallodithiolates as ligands in coordination, bioinorganic, and organometallic chemistry. Chem Rev. 2015; 115:5248–5273. [PubMed: 25948147]
21. Ogo S, et al. A functional [NiFe] hydrogenase mimic that catalyzes electron and hydride transfer from H_2. Science. 2013; 339:682–684. [PubMed: 23393260]
22. Barton BE, Rauchfuss TB. Hydride-containing models for the active site of the nickel−iron hydrogenases. J Am Chem Soc. 2010; 132:14877–14885. [PubMed: 20925337]
23. Barton BE, Whaley CM, Rauchfuss TB, Gray DL. Nickel−iron dithiolato hydrides relevant to the [NiFe]-hydrogenase active site. J Am Chem Soc. 2009; 131:6942–6943. [PubMed: 19413314]
24. Vaccaro L, Artero V, Canaguier S, Fontecave M, Field MJ. Mechanism of hydrogen evolution catalyzed by NiFe hydrogenases: Insights from a Ni-Ru model compound. Dalton Trans. 2010; 39:3043–3049. [PubMed: 20221538]
25. Simmons TR, Artero V. Catalytic hydrogen oxidation: Dawn of a new iron age. Angew Chem Int Ed. 2013; 52:6143–6145.
26. Chambers GM, et al. Models of the Ni-L and Ni-SI_a states of the [NiFe]-hydrogenase active site. Inorg Chem. 2016; 55:419–431. [PubMed: 26421729]
27. Gennari M, et al. Influence of mixed thiolate/thioether versus dithiolate coordination on the accessibility of the uncommon +I and +III oxidation states for the nickel ion: An experimental and computational study. Inorg Chem. 2011; 50:3707–3716. [PubMed: 21428312]
28. Gennari M, et al. Reversible apical coordination of imidazole between the Ni(III) and Ni(II) oxidation states of a dithiolate complex: A process related to the Ni superoxide dismutase. Inorg Chem. 2010; 49:6399–6401. [PubMed: 20553029]
29. Canaguier S, et al. A structural and functional mimic of the active site of NiFe hydrogenases. Chem Commun. 2010; 46:5876–5878.
30. Zhu W, et al. Modulation of the electronic structure and the Ni–Fe distance in heterobimetallic models for the active site in [NiFe] hydrogenase. Proc Natl Acad Sci U S A. 2005; 102:18280–18285. [PubMed: 16352727]
31. Darensbourg DJ, Reibenspies JH, Lai C-H, Lee W-Z, Darensbourg MY. Analysis of an organometallic iron site model for the heterodimetallic unit of [NiFe] hydrogenase. J Am Chem Soc. 1997; 119:7903–7904.

32. Pandelia M-E, Ogata H, Lubitz W. Intermediates in the catalytic cycle of [NiFe] hydrogenase: Functional spectroscopy of the active site. ChemPhysChem. 2010; 11:1127–1140. [PubMed: 20301175]
33. Roncaroli F, et al. Cofactor composition and function of a H_2-sensing regulatory hydrogenase as revealed by Mossbauer and EPR spectroscopy. Chem Sci. 2015; 6:4495–4507.
34. Lubitz, W., Gastel, MV., Gärtner, W. Nickel and its surprising impact in nature. Sigel, A.Sigel, H., Sigel, RKO., editors. John Wiley &Sons Ltd; 2007. p. 279-322.
35. Roy S, Groy TL, Jones AK. Biomimetic model for [FeFe]-hydrogenase: Asymmetrically disubstituted diiron complex with a redox-active 2,2'-bipyridyl ligand. Dalton Trans. 2013; 42:3843–3853. [PubMed: 23307026]
36. Farmer PJ, Reibenspies JH, Lindahl PA, Darensbourg MY. Effects of sulfur site modification on the redox potentials of derivatives of [N,N'-bis(2-mercaptoethyl)-1,5-diazacyclooctanato]nickel(II). J Am Chem Soc. 1993; 115:4665–4674.
37. Izutsu, K. Acid-base dissociation constants in dipolar aprotic solvents. Blackwell Scientific; 1990.
38. Costentin C, Drouet S, Robert M, Savéant J-M. Turnover numbers, turnover frequencies, and overpotential in molecular catalysis of electrochemical reactions. Cyclic voltammetry and preparative-scale electrolysis. J Am Chem Soc. 2012; 134:11235–11242. [PubMed: 22670885]
39. Artero V, Savéant J-M. Toward the rational benchmarking of homogeneous H_2-evolving catalysts. Energy Environ Sci. 2014; 7:3808–3814. [PubMed: 26269710]
40. Costentin C, Dridi H, Savéant J-M. Molecular catalysis of H_2 evolution: Diagnosing heterolytic versus homolytic pathways. J Am Chem Soc. 2014; 136:13727–13734. [PubMed: 25190347]
41. Sampson MD, Kubiak CP. Electrocatalytic dihydrogen production by an earth-abundant manganese bipyridine catalyst. Inorg Chem. 2015; 54:6674–6676. [PubMed: 26125125]
42. Shaw WJ, Helm ML, DuBois DL. A modular, energy-based approach to the development of nickel containing molecular electrocatalysts for hydrogen production and oxidation. Biochim Biophys Acta Bioenerg. 2013; 1827:1123–1139.
43. van der Meer M, Glais E, Siewert I, Sarkar B. Electrocatalytic dihydrogen production with a robust mesoionic pyridylcarbene cobalt catalyst. Angew Chem Int Ed. 2015; 54:13792–13795.
44. Kampa M, Pandelia M-E, Lubitz W, van Gastel M, Neese F. A metal–metal bond in the light-induced state of [NiFe] hydrogenases with relevance to hydrogen evolution. J Am Chem Soc. 2013; 135:3915–3925. [PubMed: 23402569]
45. Perotto CU, et al. A Ni(I)Fe(II) analogue of the Ni-L state of the active site of the [NiFe] hydrogenases. Chem Commun. 2015; 51:16988–16991.
46. Yoo C, Oh S, Kim J, Lee Y. Transmethylation of a four-coordinate nickel(I) monocarbonyl species with methyl iodide. Chem Sci. 2014; 5:3853–3858.
47. Greene BL, Wu C-H, McTernan PM, Adams MWW, Dyer RB. Proton-coupled electron transfer dynamics in the catalytic mechanism of a [NiFe]-hydrogenase. J Am Chem Soc. 2015; 137:4558–4566. [PubMed: 25790178]
48. Matson EM, et al. Nickel(II) pincer carbene complexes: Oxidative addition of an aryl C–H bond to form a Ni(II) hydride. Organometallics. 2015; 34:399–407.
49. Breitenfeld J, Scopelliti R, Hu X. Synthesis, reactivity, and catalytic application of a nickel pincer hydride complex. Organometallics. 2012; 31:2128–2136.
50. Boro BJ, Duesler EN, Goldberg KI, Kemp RA. Synthesis, characterization, and reactivity of nickel hydride complexes containing 2,6-$C_6H_3(CH_2PR_2)_2$ (R =tBu,cHex, and iPr) pincer ligands. Inorg Chem. 2009; 48:5081. [PubMed: 19456134]
51. Peters JW, et al. [FeFe]- and [NiFe]-hydrogenase diversity, mechanism, and maturation. BBA-Mol Cell Res. 2015; 1853:1350–1369.
52. Adamska A, et al. Identification and characterization of the "super-reduced" state of the H-cluster in FeFe hydrogenase: A new building block for the catalytic cycle? Angew Chem Int Ed. 2012; 51:11458–11462.
53. Chernev P, et al. Hydride binding to the active site of [FeFe]-hydrogenase. Inorg Chem. 2014; 53:12164–12177. [PubMed: 25369169]

54. Ezzaher S, et al. Evidence for the formation of terminal hydrides by protonation of an asymmetric iron hydrogenase active site mimic. Inorg Chem. 2007; 46:3426–3428. [PubMed: 17397148]
55. Mealli C, Rauchfuss TB. Models for the hydrogenases put the focus where it should be-hydrogen. Angew Chem Int Ed. 2007; 46:8942–8944.
56. Barton BE, Olsen MT, Rauchfuss TB. Aza- and oxadithiolates are probable proton relays in functional models for the FeFe-hydrogenases. J Am Chem Soc. 2008; 130:16834–16835. [PubMed: 19053433]
57. Olsen MT, Rauchfuss TB, Wilson SR. Role of the azadithiolate cofactor in models for FeFe-hydrogenase: Novel structures and catalytic implications. J Am Chem Soc. 2010; 132:17733–17740. [PubMed: 21114298]
58. Carroll ME, Barton BE, Rauchfuss TB, Carroll PJ. Synthetic models for the active site of the FeFe-hydrogenase: Catalytic proton reduction and the structure of the doubly protonated intermediate. J Am Chem Soc. 2012; 134:18843–18852. [PubMed: 23126330]
59. Zaffaroni R, Rauchfuss TB, Gray DL, De Gioia L, Zampella G. Terminal vs bridging hydrides of diiron dithiolates: Protonation of Fe_2(dithiolate)$(CO)_2(PMe_3)_4$. J Am Chem Soc. 2012; 134:19260–19269. [PubMed: 23095145]
60. Camara JM, Rauchfuss TB. Combining acid-base, redox and substrate binding functionalities to give a complete model for the FeFe -hydrogenase. Nature Chem. 2012; 4:26–30.
61. Reger DL, Coleman C. Preparation and reactions of the (dicarbonyl)(η^5-cyclopentadienyl)(tetrahydrofuran)iron cation: A convenient route to (dicarbonyl)(η^5-cyclopentadiemyl)(η^2-olefin)iron cations and related complexes. J Organomet Chem. 1977; 131:153–162.
62. Bhugun I, Lexa D, Savéant J-M. Homogeneous catalysis of electrochemical hydrogen evolution by iron(0) porphyrins. J Am Chem Soc. 1996; 118:3982–3983.

Europe PMC Funders Author Manuscripts

Europe PMC Funders Author Manuscripts

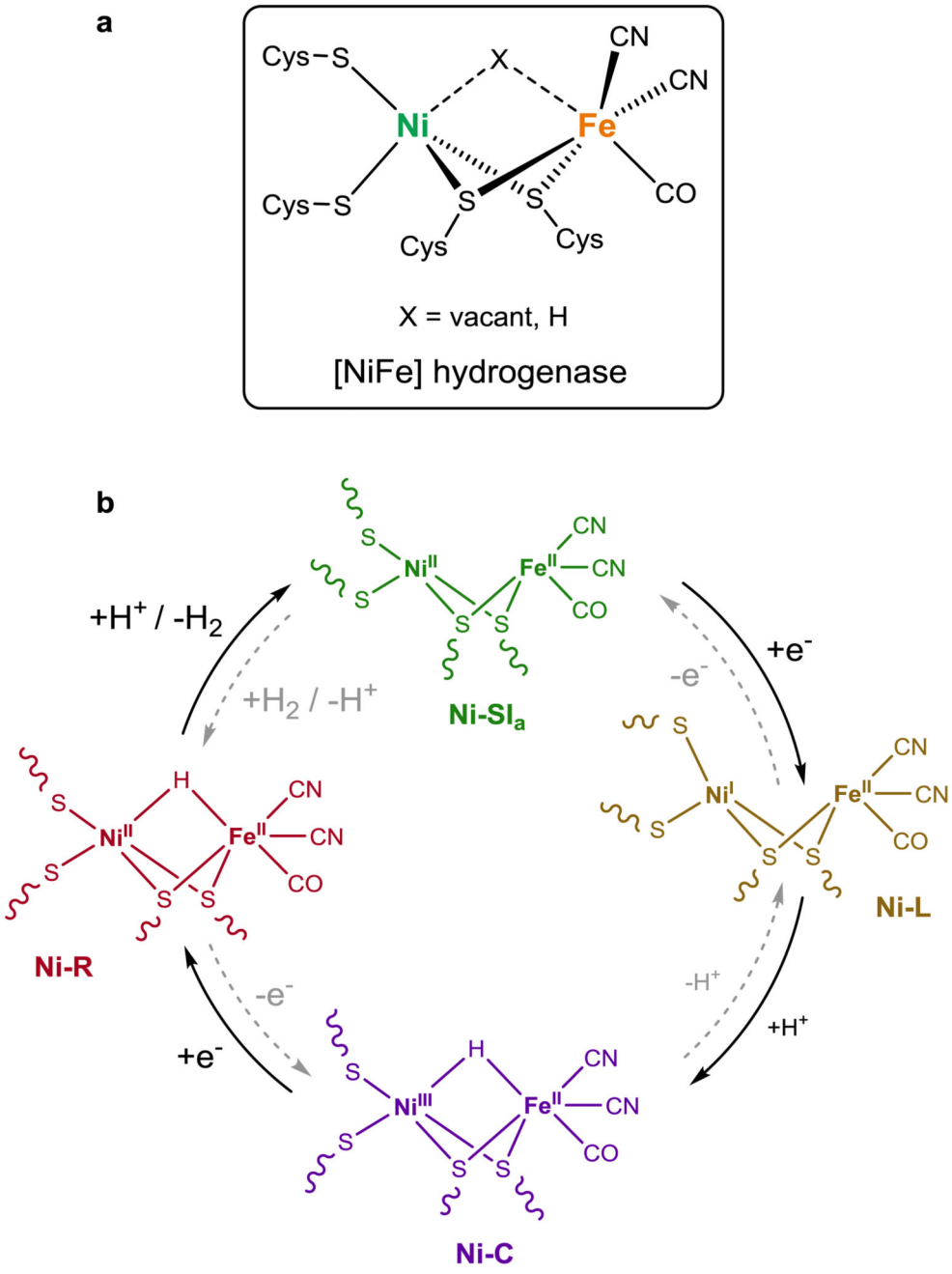

Figure 1. Active site and H_2 production catalytic cyclic of the [NiFe] hydrogenase.

a, Schematic representation of the active site of [NiFe] hydrogenase. **b,** Currently accepted mechanism for H_2 evolution(/oxidation).[2,6,8,9,47] After a first reduction, followed by proton transfer, the diamagnetic Ni-SI_a state ($Ni^{II}Fe^{II}$) is converted into a paramagnetic metal-hydride species, Ni-C ($Ni^{III}\mu(H)Fe^{II}$). The paramagnetic Ni-L state ($Ni^{I}Fe^{II}$) has been proposed to be an active intermediate between Ni-SI_a and Ni-C. Ni-C is then further reduced to form the diamagnetic Ni-R species ($Ni^{II}\mu(H)Fe^{II}$). Protonation of Ni-R allows to generate H_2 heterolytically and to restore Ni-SI_a.

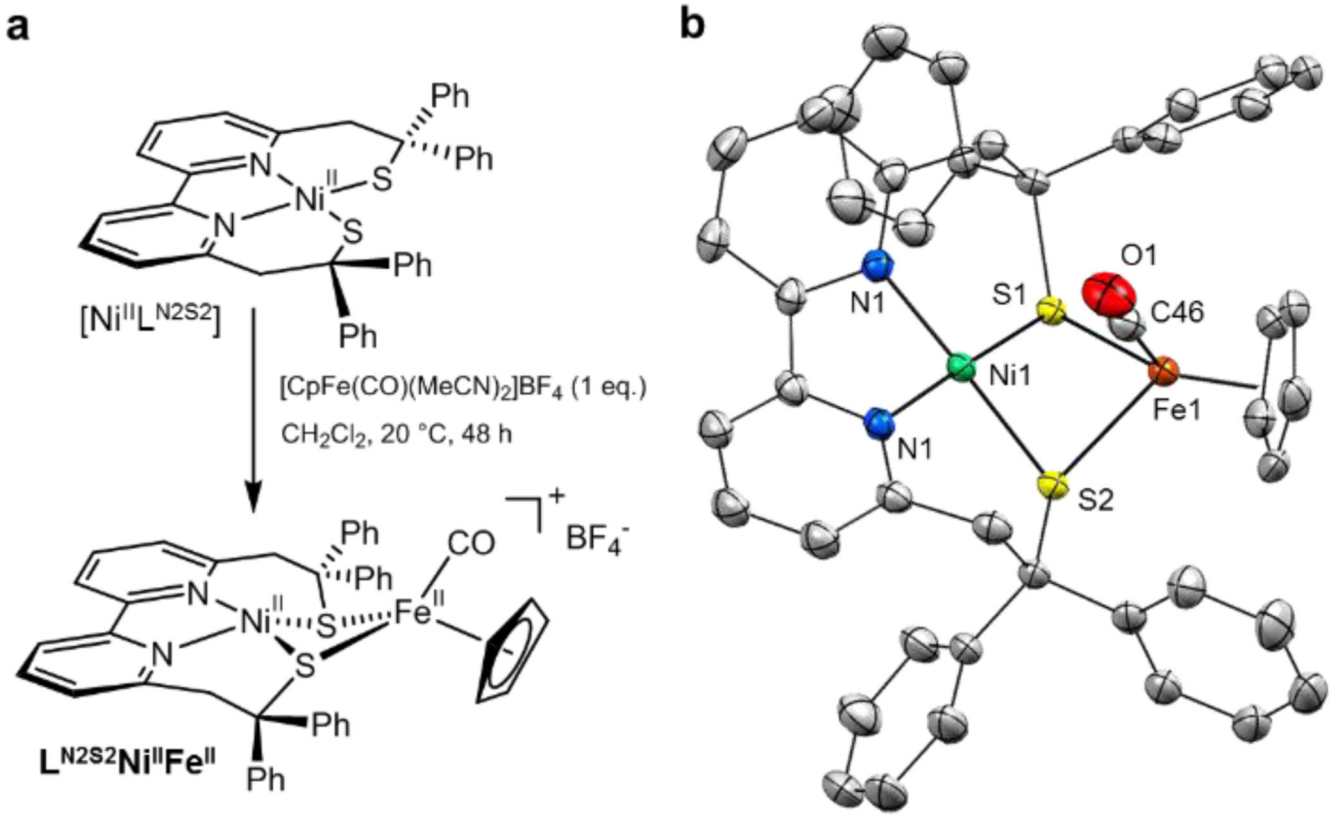

Figure 2. Synthesis and X-ray structure of $L^{N2S2}Ni^{II}Fe^{II}$.

a, Synthetic procedure for $[L^{N2S2}Ni^{II}Fe^{II}]BF_4$ ($\mathbf{L^{N2S2}Ni^{II}Fe^{II}}BF_4$). **b,** ORTEP view of only one crystallographically independent unit of the $\mathbf{L^{N2S2}Ni^{II}Fe^{II}}$ cation (50% thermal ellipsoids). The structure of $\mathbf{L^{N2S2}Ni^{II}Fe^{II}}$ is similar to the Ni-Si_a state of the [NiFe] hydrogenase with an identical {$NiFeS_2$} core and a Ni···Fe distance of 2.88(4) Å close to that (~2.8 Å) determined for Ni-SI_a.

Europe PMC Funders Author Manuscripts

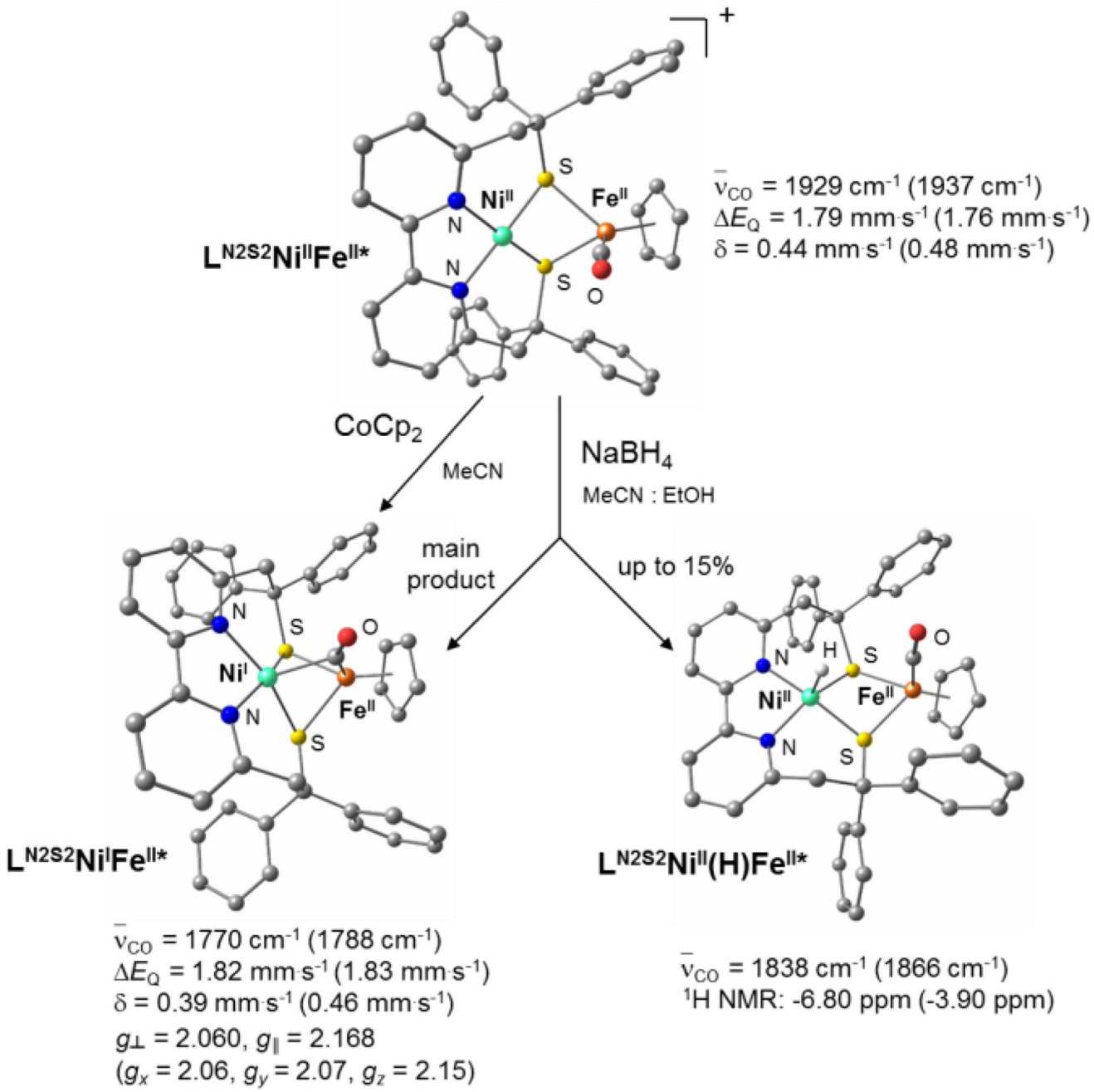

Figure 3. DFT-optimized structures and principal spectroscopic characterizations of $L^{N2S2}Ni^{II}Fe^{II}$, $L^{N2S2}Ni^{I}Fe^{II}$ and $L^{N2S2}Ni^{II}(H)Fe^{II}$.

Reaction of $\mathbf{L^{N2S2}Ni^{II}Fe^{II}}$ with $CoCp_2$ affords $\mathbf{L^{N2S2}Ni^{I}Fe^{II}}$, a mimic of the Ni-L state of the [NiFe] hydrogenase. When $\mathbf{L^{N2S2}Ni^{II}Fe^{II}}$ is reacted with $NaBH_4$, even if the main product is the reduced species ($\mathbf{L^{N2S2}Ni^{I}Fe^{II}}$), up to a 15% of the metal-hydride complex $\mathbf{L^{N2S2}Ni^{II}(H)Fe^{II}}$ is also formed. The latter, with a Ni-H distance of 1.55 Å, is a model of the Ni-R state of the enzyme ($d_{Ni\text{-}H}$ = 1.58 Å). Asterisks indicate that DFT-optimized

structures are shown. The experimental spectroscopic parameters are indicated for the different species with the corresponding calculated values into brackets.

Europe PMC Funders Author Manuscripts

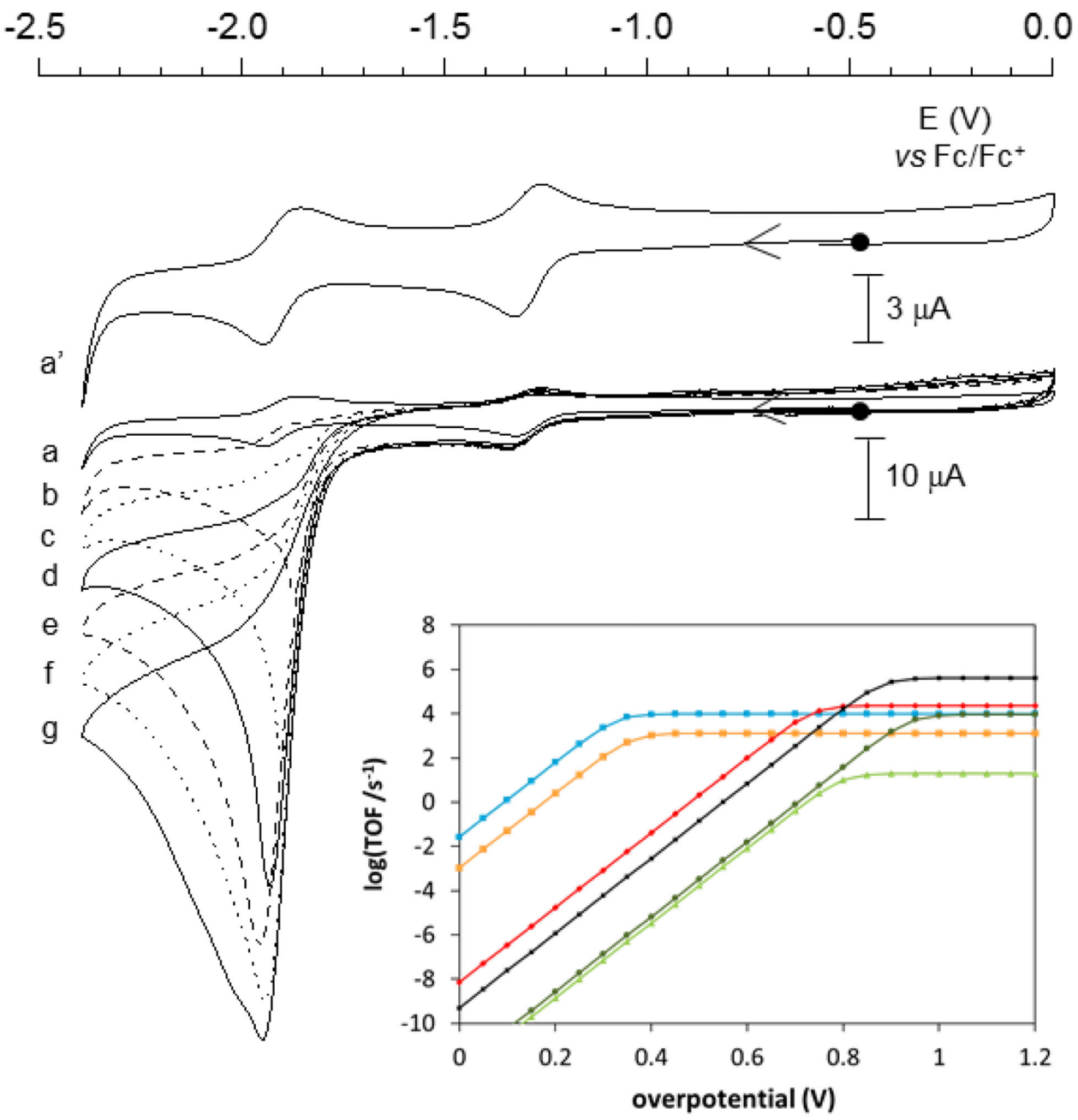

Figure 4. Electrocatalytic properties for H_2 production of $L^{N2S2}Ni^{II}Fe^{II}$.

CVs of $L^{N2S2}Ni^{II}Fe^{II}$ (0.20 mM) before (a and a') and after (b-g) addition of various amounts of Et_3NHBF_4 in MeCN solution, 0.1 M n-Bu_4NClO_4, on a glassy carbon electrode at 100 mV s^{-1}: (b) 5 equiv.; (c) 10 equiv.; (d) 15 equiv.; (e) 20 equiv.; (f) 25 equiv; (g) 30 equiv. Upon addition of Et_3NHBF_4 a catalytic wave corresponding to the reduction of protons into H_2 develops at E_{cat} = –1.90 V vs Fc^+/Fc, i.e. on the top of the second reversible process of the complex. The inset displays catalytic Tafel plots relating turnover frequency and driving force of H_2 evolution, and allows benchmarking the performances of

Europe PMC Funders Author Manuscripts

$\mathbf{L^{N2S2}Ni^{II}Fe^{II}}$ with previously reported H_2-evolving electrocatalysts: $\mathbf{L^{N2S2}Ni^{II}Fe^{II}}BF_4$ (red); [Mn(mesbpy)$(CO)_3$(MeCN)](OTf) (mesbpy=6,6'-dimesityl-2,2'- bipyridine) (dark green);[6] [Ni(xbsms)Mn$(CO)_3(H_2O)]^+$ (xbsms a S4 donor ligand) (light green);41 FeTPP(black);14,39,62 $[Ni^{II}(P_2^{Ph}N_2^{C6H4X})_2]^{2+}$ (X= $CH_2P(O)$) (orange);39 $Co^{II}(dmgH)_2$py (blue).39 The $\mathbf{L^{N2S2}Ni^{II}Fe^{II}}$ complex displays significant catalytic activity (log(TOF)/ s^{-1})>1) for overpotentials >500 mV, rivalling other biomimetic dinuclear electrocatalysts.

Europe PMC Funders Author Manuscripts

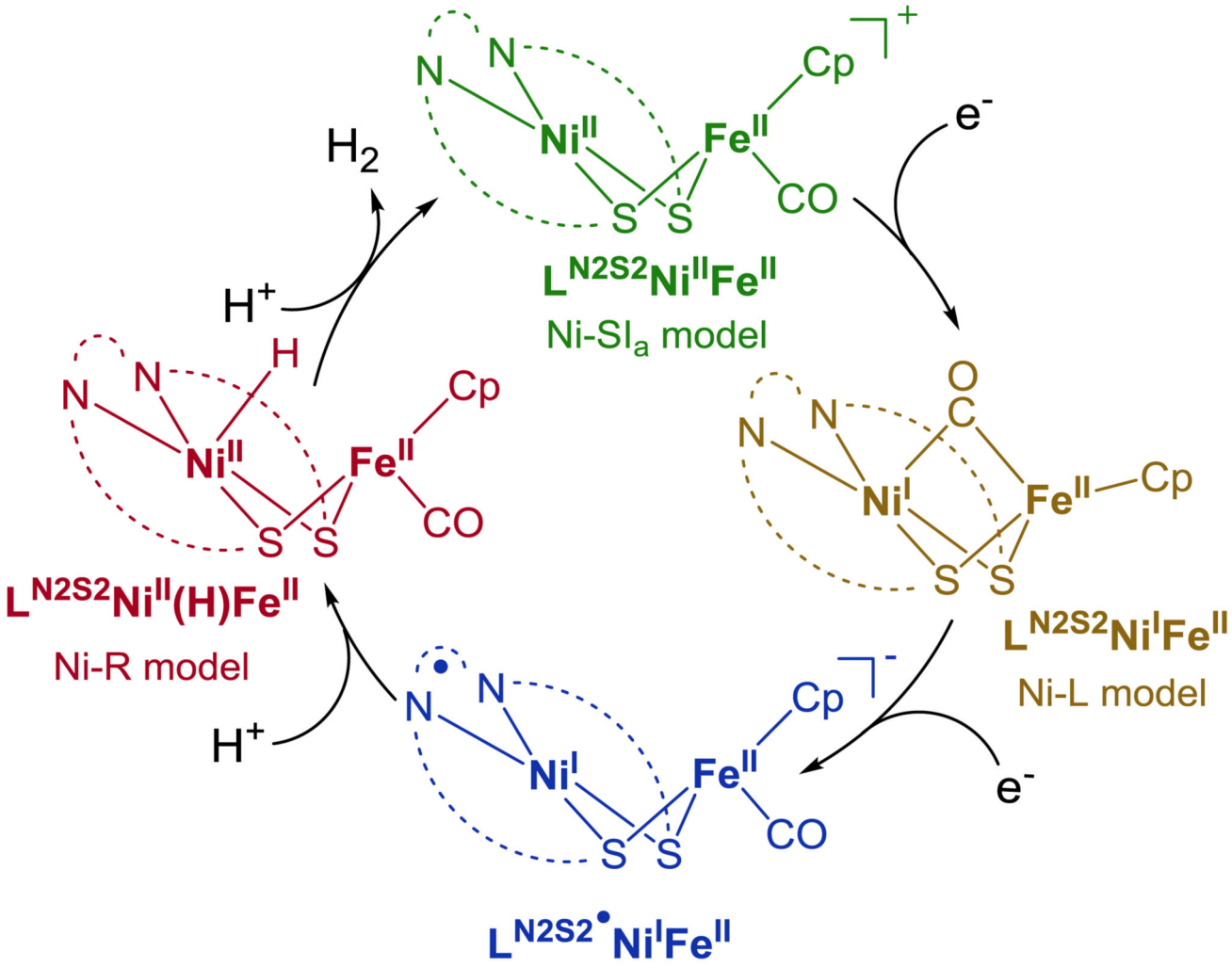

Figure 5. H_2 production catalytic cycle of $L^{N2S2}Ni^{II}Fe^{II}$.

Proposed catalytic pathway for H_2 evolution mediated by $\mathbf{L^{N2S2}Ni^{II}Fe^{II}}$ at the catalytic wave. After a one-electron reduction, $\mathbf{L^{N2S2}Ni^{II}Fe^{II}}$ generates $\mathbf{L^{N2S2}Ni^{I}Fe^{II}}$, a mimic of the Ni-L state, which is then further reduced to afford the metal-radical complex $\mathbf{L^{N2S2\bullet}Ni^{I}Fe^{II}}$. The latter reacts with protons to yield the metal-hydride complex $\mathbf{L^{N2S2}Ni^{II}(H)Fe^{II}}$, a model of Ni-R, which is protonated to produce H_2 with concomitant regeneration of the initial $\mathbf{L^{N2S2}Ni^{II}Fe^{II}}$ complex.